

Anionic Mixed Thiolate–Sulfide-Bridged Roussin’s Red Esters [(NO)₂Fe(μ-SR)(μ-S)Fe(NO)₂][−] (R = Et, Me, Ph): A Key Intermediate for Transformation of Dinitrosyl Iron Complexes (DNICs) to [2Fe-2S] Clusters

Tsai-Te Lu, Hsiao-Wen Huang, and Wen-Feng Liaw*

Department of Chemistry, National Tsing Hua University, Hsinchu 30013, Taiwan

Received July 2, 2009

Transformations of dinitrosyl iron complex (DNIC) [(NO)₂Fe(SEt)₂][−] and the anionic Roussin’s red ester (RRE) [(NO)₂Fe(μ-SEt)₂Fe(NO)₂][−] into [2Fe-2S] clusters facilitated by HSCPh₃/Me₂S₃ and [Fe(SEt)₄][−], respectively, via an intermediate anionic mixed thiolate–sulfide-bridged RRE [(NO)₂Fe(μ-SEt)(μ-S)Fe(NO)₂][−] through the reassembling process [(NO)₂Fe(SEt)₂][−] (**2**)/[(NO)₂Fe(μ-SEt)₂Fe(NO)₂][−] (**4**) → [(NO)₂Fe(μ-SEt)(μ-S)Fe(NO)₂][−] (**3-Et**) → [(NO)₂Fe(μ-S)₂Fe(NO)₂]^{2−} (**5**) → [(SEt)₂Fe(μ-S)₂Fe(SEt)₂]^{2−} (**1**) were demonstrated. The anionic mixed thiolate–sulfide-bridged RRE **3-Et** was characterized by IR, UV–vis, electron paramagnetic resonance, ¹H NMR, cyclic voltammetry, and single-crystal X-ray diffraction. In contrast to the nucleophilicity displayed by complex **2**, the inertness of [(NO)₂Fe(SPh)₂][−] toward HSCPh₃ implicates how the reducing ability of the coordinated thiolates of DNICs modulate the release of sulfide from HSCPh₃ via reduction and the conversion of DNICs into the anionic mixed sulfide–thiolate-bridged complex. The reversible interconversion between complex **3-Et** and complex [(NO)₂Fe(μ-SPh)(μ-S)Fe(NO)₂][−] (**3-Ph**) via protonation and a bridged-thiolate exchange reaction, respectively, demonstrates that the {Fe(NO)₂}⁹–{Fe(NO)₂}⁹ motif displays a preference for the stronger electron-donating alkylthiolate-bridged ligand over the phenylthiolate-bridged ligand. This study may signify that the anionic mixed thiolate–sulfide-bridged RREs act as a key intermediate in the transformation of DNICs into [2Fe–2S] clusters. Also, the thiolate-coordinate DNICs serve as not only the thiolate/electron carrier activating the incorporation of sulfide of HSCPh₃ (Me₂S₃) to assemble the [Fe(μ-S)₂Fe] core but also the Fe source in the biosynthesis of the [2Fe–2S] and [4Fe–4S] iron–sulfur clusters.

Introduction

Nitric oxide modulates versatile physiological reactions by nitrosylation of various nonheme Fe-containing proteins,

leading to dinitrosyl iron complexes (DNICs) with an electron paramagnetic resonance (EPR) signal at *g* = 2.03, for example, modulating cellular iron homeostasis, altering the metabolism of bacteria, regulating the expression of genes to detoxify reactive nitrogen species (RNS) or repair/regenerate essential [Fe–S] proteins,^{1–3} and lowering the activity of human and mouse ferroxidase to prevent the invading pathogens from absorbing the heme/Fe source.⁴ In *Escherichia coli*, degradation of the [2Fe–2S] cluster of SoxR by nitric oxide yielding DNICs stimulates the expression of SoxS to trigger the expression of proteins involved in detoxifying RNS.^{3a} Of importance, DNICs derived from the nitrosylation of Fe-storage protein (i.e., mammalian ferritin, cellular labile/chelatable iron pool, or [Fe–S] cluster-containing proteins) were actively delivered between cells via multidrug resistance-associated protein 1 in the form of glutathione-coordinated DNICs (DNIC-GSH).^{1c,d,5} Also, DNICs were found to exert NO-related functions, such as S-nitrosation of

*To whom correspondence should be addressed. E-mail: wliaw@mx.nthu.edu.tw.

(1) (a) Toledo, J. C.; Bosworth, C. A., Jr.; Hennon, S. W.; Mahtani, H. K.; Bergonia, H. A.; Lancaster, J. R., Jr. *J. Biol. Chem.* **2008**, *283*, 28926–28933. (b) Lewandowska, H.; Meczynska, S.; Sochanowicz, B.; Sadlo, J.; Kruszewski, M. *J. Biol. Inorg. Chem.* **2007**, *12*, 345–352. (c) Watts, R. N.; Hawkins, C.; Ponka, P.; Richardson, D. R. *Proc. Natl. Acad. Sci.* **2006**, *103*, 7670–7675. (d) Richardson, D. R.; Lok, H. C. *Biochem. Biophys. Acta* **2008**, *1780*, 638–651.

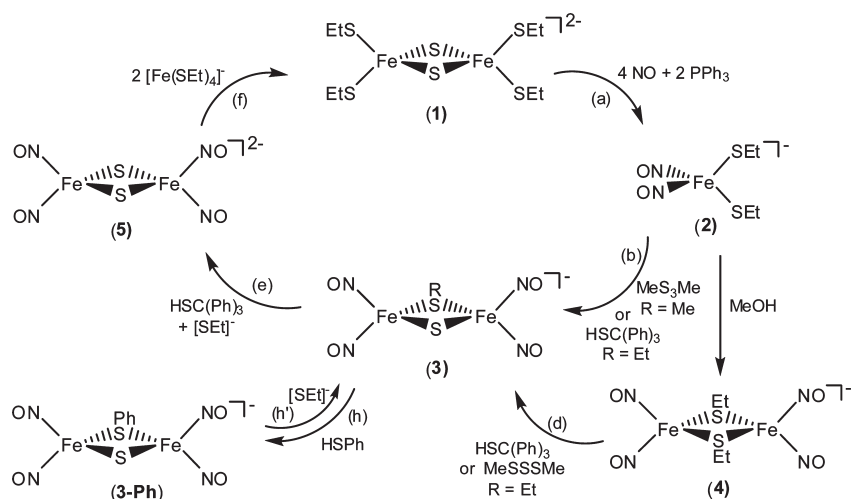
(2) (a) Pullan, S. T.; Gidley, M. D.; Jones, R. A.; Barret, J.; Stevanin, T. M.; Read, R. C.; Freen, J.; Poole, R. K. *J. Bacteriol.* **2007**, *189*, 1845–1855. (b) Singh, A.; Guidry, L.; Narasimhulu, K. V.; Mai, D.; Trombley, J.; Redding, K. E.; Giles, G. I.; Lancaster, J. R.; Steyn, A. J. C. *Proc. Natl. Acad. Sci.* **2007**, *104*, 11562–11567.

(3) (a) Ding, H.; Hidalgo, E.; Demple, B. *J. Biol. Chem.* **1996**, *271*, 33173–33175. (b) Cruz-Ramos, H.; Crack, J.; Wu, G.; Hughes, N. M.; Scott, C.; Thomson, J. A.; Green, J.; Poole, R. K. *EMBO J.* **2002**, *21*, 3235–3244. (c) Nakano, M. M.; Geng, H.; Nakano, S.; Kobayashi, K. *J. Bacteriol.* **2006**, *188*, 5878–5887. (d) Yuki, E. T.; Elbaz, M. A.; Nakano, M. M.; Moenne-Loccoz, P. *Biochemistry* **2008**, *47*, 13084–13092. (e) Jones-Carson, J.; Laughlin, J.; Hamad, M. A.; Stewart, A. L.; Voskuil, M. I.; Vazquez-Torres, A. *PLoS ONE* **2008**, *3*, e1976.

(4) Dailey, H. A. *Biosynthesis of Heme and Chlorophylls*; McGraw-Hill: New York, 1990; pp 123–161.

(5) Lee, M.; Arosio, P.; Cozzi, A.; Chasteen, N. D. *Biochemistry* **1994**, *33*, 3679–3687.

Scheme 1



bovine serum albumin or activation of soluble guanylate cyclase.⁶ Interestingly, DNICs not only play a key role in the storage and transport of NO but also regulate the Fe uptake and cellular iron homeostasis by the efflux of Fe in the form of DNIC-GSH.¹

A requirement of the complex assembly machinery for the maturation of [Fe-S] proteins was identified, but the assembling mechanism remained for further investigation.⁷ It is proposed that the biosynthesis of [Fe-S] clusters includes three steps: (i) mobilizing iron and sulfur atoms from their storage sources in nontoxic forms, (ii) assembling them into an [Fe-S] core, and (iii) inserting the assembled [Fe-S] core into apoprotein.⁷⁻¹⁰ Inorganic sulfur atoms (S^0) are generated from cysteine catalyzed by cysteine desulfurase (carried by cysteine desulfurase in the form of persulfide (RS-SH)) and inserted to form an [Fe-S] core via reductive cleavage of the S-S bond by NADH mediated by Yah1 and Arh1.^{7,8} It is known that persulfide and trisulfide (RS-S-SR') were observed on IscU upon incubation with IscS and cysteine, that is, sulfur atom(s) anchored on IscU in the form of persulfide or trisulfide is proposed to incorporate with Fe to assemble [Fe-S] clusters.⁹ The Fe source for the biosynthesis of [Fe-S] clusters was proposed to derive from IscA and

frataxin, which donates Fe to IscU facilitated by cysteine and IscS.¹⁰ The donation of Fe to IscU facilitated by cysteine and IscS implicated that an [Fe-S-SR] complex was produced in the interaction of IscA, IscS, and cysteine and delivered to IscU for further assembling. A dual role of IscA was found in which it acts as a scaffold protein by anchoring one [2Fe-2S] cluster in the interface of two IscA monomers.^{10d}

In biological systems, NO-modified [2Fe-2S]/[4Fe-4S] clusters in mitochondrial aconitase, HiPIP, and SoxR, that is, DNICs and anionic Roussin's red esters (RREs), were automatically transformed into the original [2Fe-2S]/[4Fe-4S] clusters in aerobically growing *E. coli* with no new protein synthesis.^{11,12} Also, DNICs can be directly transformed back to the ferredoxin [2Fe-2S] cluster by cysteine desulfurase (IscS) and L-cysteine in vitro with no need of the addition of iron or any other protein components in the repair of NO-modified ferredoxin [2Fe-2S] clusters.¹³

It is known that iron sulfur clusters were synthesized via the self-assembly pathway.¹⁴ Recently, the transformation of $[(NO)_2FeS_5]^-$ into $[S_5Fe(\mu-S)_2FeS_5]^{2-}$ in the presence of the NO-acceptor reagent $[(C_4H_8O)Fe(S,S-C_6H_4)_2]^-$ by photolysis was reported.^{15a} Conversion of DNICs into [4Fe-4S] clusters in the presence of $[Fe(SR)_4]^-$ and S_8 was also demonstrated in a biomimetic model study.^{15b} Also, degradation of [2Fe-2S] clusters ligated by aromatic thiolates via nitrosylation was found to generate DNICs with elimination of the elemental sulfur atoms.¹⁶ In this report, we attempt to adopt

(6) (a) Boese, M.; Mordvintcev, P. I.; Vanin, A. F.; Busse, R.; Mülsch, A. *J. Biol. Chem.* **1995**, *270*, 29244-29249. (b) Mülsch, A.; Mordvintcev, P.; Vanin, A. F.; Busse, R. *FEBS Lett.* **1991**, *294*, 252-256. (c) Giannone, G.; Takeda, K.; Kleschyov, A. L. *J. Physiol.* **2000**, *529*, 735-745. (d) Severina, I. S.; Bussygina, G. O.; Pyatakova, V. N.; Malenkova, V. I.; Vanin, A. F. *Nitric Oxide* **2003**, *8*, 155-163. (e) Vasil'eva, S. V.; Osipov, A. N.; Sanina, N. A.; Aldoshin, S. M. *Dokl. Biochem. Biophys.* **2007**, *414*, 102-105. (f) Kleschyov, A. L.; Strand, S.; Schmitt, S.; Gottfried, D.; Skatchkov, M.; Sjakste, N.; Daiber, A.; Umansky, V.; Munzel, T. *Free Radical Biol. Med.* **2006**, *40*, 1340-1348.

(7) Lill, R.; Muhlenhoff, U. *Annu. Rev. Biochem.* **2008**, *77*, 669-700.
(8) (a) Zheng, L.; White, R. H.; Cash, V. L.; Jack, R. F.; Dean, D. R. *Proc. Natl. Acad. Sci.* **1993**, *90*, 2754-2758. (b) Agar, J. N.; Zheng, L.; Cash, V. L.; Dean, D. R.; Johnson, M. K. *J. Am. Chem. Soc.* **2000**, *122*, 2136-2137. (c) Agar, J. N.; Krebs, C.; Frazzon, J.; Huynh, B. H.; Dean, D. R.; Johnson, M. K. *Biochemistry* **2000**, *39*, 7856-7862.

(9) (a) Smith, A. D.; Frazzon, J.; Dean, D. R.; Johnson, M. K. *FEBS Lett.* **2005**, *579*, 5236-5240. (b) Smith, A. D.; Agar, J. N.; Johnson, K. A.; Frazzon, J.; Amster, I. J.; Dean, D. R.; Johnson, M. K. *J. Am. Chem. Soc.* **2001**, *123*, 11103-11104.

(10) (a) Yoon, T.; Cowan, J. A. *J. Am. Chem. Soc.* **2003**, *125*, 6078-6084. (b) Ding, H.; Clark, R. J.; Ding, B. *J. Biol. Chem.* **2004**, *279*, 37499-37504. (c) Ding, H.; Clark, R. J. *Biochem. J.* **2004**, *379*, 433-440. (d) Morimoto, K.; Yamashita, E.; Kondou, Y.; Lee, S. J.; Arisaka, F.; Tsukihara, T.; Nakai, M. *J. Mol. Biol.* **2006**, *360*, 117-132.

(11) (a) Kennedy, M. C.; Anthonline, E. W.; Beinert, H. *J. Biol. Chem.* **1997**, *272*, 20340-20347. (b) Foster, M. W.; Cowan, J. A. *J. Am. Chem. Soc.* **1999**, *121*, 4093-4100. (c) Ding, H.; Demple, B. *Proc. Natl. Acad. Sci. U.S.A.* **2000**, *97*, 5146-5150. (d) Tsou, C.-C.; Lu, T.-T.; Liaw, W.-F. *J. Am. Chem. Soc.* **2007**, *129*, 12626-12627.

(12) Bouton, C.; Chauveau, M.-J.; Lazereg, S.; Drapier, J.-C. *J. Biol. Chem.* **2002**, *277*, 31220-31227.

(13) Yang, W.; Rogers, P. A.; Ding, H. *J. Biol. Chem.* **2002**, *277*, 12868-12873.

(14) (a) Rao, P. V.; Holm, R. H. *Chem. Rev.* **2004**, *104*, 527-559. (b) Ohki, Y.; Sunada, Y.; Honada, M.; Katada, M.; Tatsumi, K. *J. Am. Chem. Soc.* **2003**, *125*, 4052-4053. (c) Ohki, Y.; Ikagawa, Y.; Tatsumi, K. *J. Am. Chem. Soc.* **2007**, *129*, 10457-10465.

(15) (a) Tsai, M.-L.; Chen, C.-C.; Hsu, I.-J.; Ke, S.-C.; Hsieh, C.-H.; Chiang, K.-A.; Lee, G.-H.; Wang, Y.; Chen, J.-M.; Lee, J.-F.; Liaw, W.-F. *Inorg. Chem.* **2004**, *43*, 5159-5167. (b) Tsou, C.-C.; Lin, Z.-S.; Lu, T.-T.; Liaw, W.-F. *J. Am. Chem. Soc.* **2008**, *130*, 17154-17160.

(16) Harrop, T. C.; Tonzetich, Z. J.; Reisner, E.; Lippard, S. J. *J. Am. Chem. Soc.* **2008**, *130*, 15602-15610.

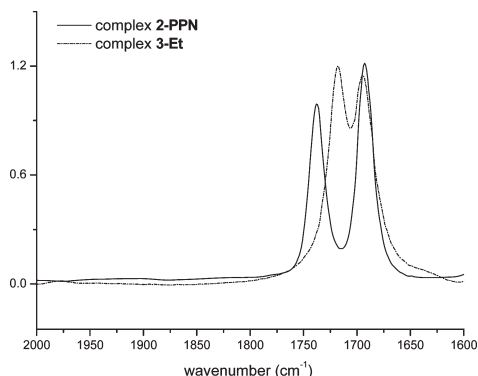


Figure 1. Infrared ν_{NO} absorbance changes for the reaction of **2-PPN** with HSCPh_3 in a 2:1 stoichiometry in CH_3CN at ambient temperature. The solid line curve (—) corresponds to **2-PPN**, and the dashed line curve (---) corresponds to the formation of complex **3-Et**.

the biomimetic model study to unravel the conversion of the NO-modified $[\text{Fe}-\text{S}]$ cluster into the $[\text{2Fe}-\text{2S}]$ cluster. Specifically, the addition of Me_2S_3 (or HSCPh_3) to $[(\text{NO})_2\text{Fe}(\text{SEt})_2]^-$ results in the formation of anionic mixed thiolate-sulfide-bridged Roussin's red ester $[(\text{NO})_2\text{Fe}(\mu\text{-SEt})(\mu\text{-S})\text{Fe}(\text{NO})_2]^-$, which was characterized by IR, UV-vis spectroscopy, ^1H NMR, and single-crystal X-ray crystallography. The anionic mixed thiolate-sulfide-bridged Roussin's red ester acts as a key intermediate in the transformation of DNICs/anionic RREs into $[\text{2Fe}-\text{2S}]$ clusters facilitated by HSCPh_3 (Me_2S_3) via the reassembling process $[(\text{NO})_2\text{Fe}(\text{SEt})_2]^-/[(\text{NO})_2\text{Fe}(\mu\text{-SEt})(\mu\text{-S})\text{Fe}(\text{NO})_2]^- \rightarrow [(\text{NO})_2\text{Fe}(\mu\text{-SEt})(\mu\text{-S})\text{Fe}(\text{NO})_2]^- \rightarrow [(\text{NO})_2\text{Fe}(\mu\text{-S})_2\text{Fe}(\text{NO})_2]^{2-} \rightarrow [(\text{SEt})_2\text{Fe}(\mu\text{-S})_2\text{Fe}(\text{SEt})_2]^{2-}$.

Results

Nitrosylation of $[(\text{SEt})_2\text{Fe}(\mu\text{-S})_2\text{Fe}(\text{SEt})_2]^{2-}$ (1**) and Transformation of $[\text{PPN}][(\text{NO})_2\text{Fe}(\text{SEt})_2]$ (**2-PPN**)/[**K-18-crown-6-ether**] $[(\text{NO})_2\text{Fe}(\mu\text{-SEt})_2\text{Fe}(\text{NO})_2]$ (**4**) into $[\text{PPN}][(\text{NO})_2\text{Fe}(\mu\text{-SEt})(\mu\text{-S})\text{Fe}(\text{NO})_2]$ (**3-Et**).** Similar to the nitrosylation of $[(\text{SPh})_2\text{Fe}(\mu\text{-S})_2\text{Fe}(\text{SPh})_2]^{2-}$ leading to the formation of complex $[(\text{NO})_2\text{Fe}(\text{SPh})_2]^-$,^{16,17} reaction of the PPN^+ salt of complex $[(\text{SEt})_2\text{Fe}(\mu\text{-S})_2\text{Fe}(\text{SEt})_2]^{2-}$ (**1-PPN**) and 4 equiv of $\text{NO}_{(\text{g})}$ at 0°C under the presence of 2 equiv of PPh_3 resulted in the formation of the PPN^+ salt of complex $[(\text{NO})_2\text{Fe}(\text{SEt})_2]^-$ (**2-PPN**) and $\text{S}=\text{PPh}_3$. Products **2-PPN** and $\text{S}=\text{PPh}_3$ were characterized by the IR ν_{NO} spectrum, displaying two strong stretching bands (1722 and 1680 cm^{-1}), and the ^{31}P NMR spectrum (^{31}P NMR (CH_3CN): δ 42.70 ppm), respectively (Scheme 1a).

Treatment of **2-PPN** with half an equivalent of HSCPh_3 yielded $[\text{PPN}][(\text{NO})_2\text{Fe}(\mu\text{-SEt})(\mu\text{-S})\text{Fe}(\text{NO})_2]$ (**3-Et**) accompanied by byproducts $[\text{PPN}][\text{SEt}]$, $(\text{EtS})_2$, and $\text{HC}(\text{Ph})_3$ characterized by ^1H NMR (Scheme 1b). The shift of the ν_{NO} stretching frequencies from 1722 and 1680 cm^{-1} to 1718 and 1693 cm^{-1} (CH_3CN) also corroborated the formation of complex **3-Et** (Figure 1). In addition, the conversion of **2-PPN** to **3-Et** was also monitored by UV-vis spectrometry; the intense bands at 438 and 799 nm disappeared, accompanied by the simultaneous formation of one absorption band at 376 nm (complex **3-Et**;

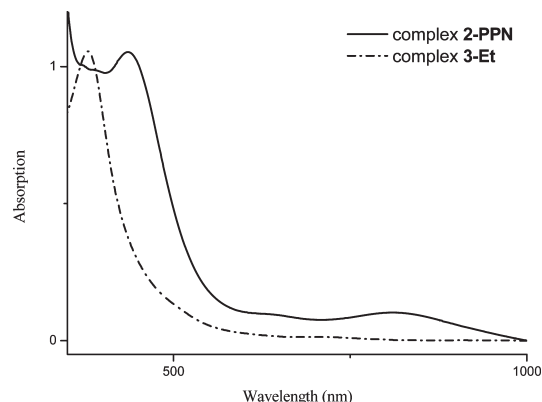


Figure 2. Conversion of **2-PPN** to complex **3-Et** monitored by UV-vis spectrometry under the addition of half an equivalent of HSCPh_3 to **2-PPN** in CH_3CN at ambient temperature. Two absorption bands at 438 and 799 nm (—) disappeared followed by the simultaneous formation of one absorption band at 376 nm (---).

Scheme 2

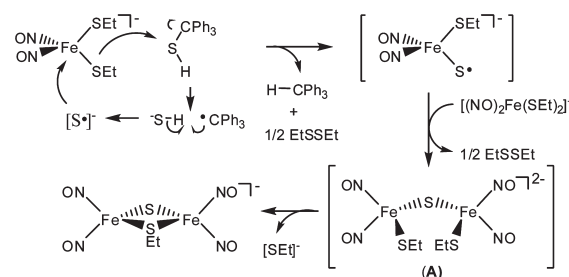


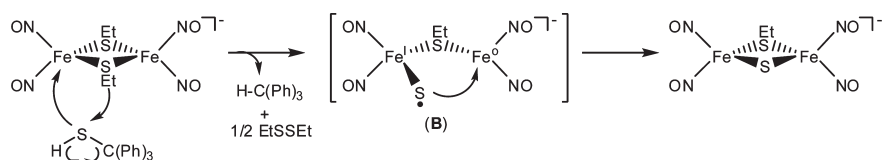
Figure 2). The ^1H NMR signal at 2.71 (q) and 1.40 (t) ppm (CD_3CN) of the ethyl group of $[\text{K-18-crown-6-ether}][(\text{NO})_2\text{Fe}(\mu\text{-SEt})(\mu\text{-S})\text{Fe}(\text{NO})_2]$ (**3-Et-K**) may rationalize the absence of an EPR signal, presumably derived from the antiferromagnetic coupling between the two $\{\text{Fe}(\text{NO})_2\}^9$ iron centers. In the previous study, **2-PPN** was demonstrated to act as a thiolate carrier and the inherent reducing species.¹⁸ This study further supports that the coordinated ethylthiolates of **2-PPN** initiated the release of sulfide from HSCPh_3 via reduction to trigger the transformation of **2-PPN** into complex **3-Et**. As shown in Scheme 2, reaction of **2-PPN** and HSCPh_3 yielding complex **3-Et** may be rationalized by the following reaction sequences: consecutive reduction of HSCPh_3 by the coordinated ethylthiolate of **2-PPN** produces the $[\text{PPN}]_2[(\text{NO})_2(\text{SEt})\text{Fe}(\mu\text{-S})\text{Fe}(\text{SEt})(\text{NO})_2]$ (**A**) intermediate along with diethyl disulfide and $\text{HC}(\text{Ph})_3$ ($E_a = -2.038\text{ V}$ (HSCPh_3), $E_a = -2.767\text{ V}$ ($[\text{EtS}]^-$),¹⁸ $E_c = -0.194\text{ V}$ ($\{\text{Fe}(\text{NO})_2\}^9/\{\text{Fe}(\text{NO})_2\}^8$ (**2-PPN**)¹⁸ vs $\text{FeCp}_2/\text{FeCp}_2^+$; Scheme 2). The subsequent elimination of the ethylthiolate of intermediate **A** affords complex **3-Et**. The biomimetic trisulfide (sulfane sulfur carrier) employed as a "S-donor species" to trigger the conversion of complex $[\text{Fe}(\text{SPh})_4]^{2-}$ into complex $[(\text{SPh})_2\text{Fe}(\mu\text{-S})_2\text{Fe}(\text{SPh})_2]^{2-}$ was reported.¹⁹ In this study, the addition of dimethyl trisulfide into **2-PPN** leading to the formation of $[\text{PPN}][(\text{NO})_2\text{Fe}(\mu\text{-SMe})(\mu\text{-S})\text{Fe}(\text{NO})_2]$ (**3-Me**) characterized by

(18) Lu, T.-T.; Tsou, C.-C.; Huang, H.-W.; Hsu, I.-J.; Chen, J.-M.; Kuo, T.-S.; Wang, Y.; Liaw, W.-F. *Inorg. Chem.* **2008**, *47*, 6040–6050.

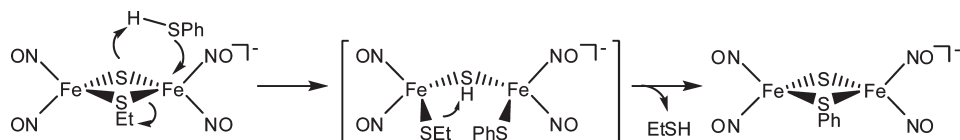
(19) Coucouvanis, D.; Swenson, D.; Stremple, P.; Baenziger, N. C. *J. Am. Chem. Soc.* **1979**, *101*, 3392–3394.

(17) Tsai, F.-T.; Chiou, S.-J.; Tsai, M.-C.; Tsai, M.-L.; Huang, H.-W.; Chiang, M.-H.; Liaw, W.-F. *Inorg. Chem.* **2005**, *44*, 5872–5881.

Scheme 3



Scheme 4



IR, UV-vis, ^1H NMR, and single-crystal X-ray structure was demonstrated.

Transformation of **2-PPN** into the neutral RRE $[(\text{NO})_2\text{Fe}(\mu\text{-SEt})_2\text{Fe}(\text{NO})_2]$ driven by $[(\text{MeOH})_n \cdots \text{SEt}]^-$ hydrogen-bonding interaction and the subsequent reduction of RRE $[(\text{NO})_2\text{Fe}(\mu\text{-SEt})_2\text{Fe}(\text{NO})_2]$ by DNIC yielding the anionic $[\text{PPN}][(\text{NO})_2\text{Fe}(\mu\text{-SEt})_2\text{Fe}(\text{NO})_2]$ were demonstrated.¹⁸ Conversion of $[\text{K-18-crown-6-ether}][(\text{NO})_2\text{Fe}(\mu\text{-SEt})_2\text{Fe}(\text{NO})_2]$ (**4**) into $[\text{K-18-crown-6-ether}][(\text{NO})_2\text{Fe}(\mu\text{-SEt})(\mu\text{-S})\text{Fe}(\text{NO})_2]$ (**3-Et-K**) under the presence of HSCPh_3 was displayed and was monitored by IR ν_{NO} spectra. The shift of NO stretching frequencies from 1673 s cm^{-1} and 1655 s cm^{-1} to 1710 s cm^{-1} and 1687 s cm^{-1} was consistent with the formation of **3-Et-K** accompanied by byproducts HC(Ph)_3 and EtSSEt identified by ^1H NMR when the THF solution of complex **4** was reacted with HSCPh_3 in a 1:1 molar ratio (Scheme 1d). The elongation of the Fe–S bond of complex **4**, compared to that of complex $[(\text{NO})_2\text{Fe}(\mu\text{-SEt})_2\text{Fe}(\text{NO})_2]$, was observed upon the reduction of complex $[(\text{NO})_2\text{Fe}(\mu\text{-SEt})_2\text{Fe}(\text{NO})_2]$.¹⁸ The electronic richness of the Fe center in complex **4** may enhance the $d\pi\text{-}\pi\pi$ repulsion to promote the thiolate reducing ability, since the theoretical computations reported in the previous study have shown that the singly-occupied molecular orbital of complex **4** is composed of both Fe atoms ($\sim 50\%$ $d_{x^2-y^2}$) and its associated S ligands (25% P_x orbitals).¹⁸ Then, the transformation of complex **4** into **3-Et-K** under the presence of HSCPh_3 may be accounted for by the following reaction sequences. As shown in Scheme 3, reduction of HSCPh_3 by the bridged ethylthiolate of the anionic RRE **4** led to the proposed intermediate **B** accompanied by the liberation of byproducts HC(Ph)_3 and diethyl disulfide ($E_{1/2}^{0/1-} = -0.95$ V (complex **4**) vs $\text{FeCp}_2/\text{FeCp}_2^+$).¹⁸ The subsequent electrophilic attack of the terminal iron-bound $[\text{S}]^-$ ligand on the neighboring iron yields **3-Et-K**. In a similar fashion, transformation of complex **4** into **3-Et-K** was also observed under the presence of 1 equiv of dimethyl trisulfide with the isolation of byproducts dimethyl disulfide and diethyl disulfide, characterized by ^1H NMR.

Compared to that of the neutral RRE $[(\text{NO})_2\text{Fe}(\mu\text{-SEt})_2\text{Fe}(\text{NO})_2]$ (ν_{NO} : 1809 vw , 1774 s , 1749 s cm^{-1}), the IR spectrum (ν_{NO} : 1718 s , 1693 s cm^{-1}) of **3-Et-K** displays a different pattern and position. Interestingly, the IR spectrum of **3-Et-K** exhibits a similar pattern to that of Roussin's red

salt (RRS) $[\text{K-18-crown-6-ether}]_2[(\text{NO})_2\text{Fe}(\mu\text{-S})_2\text{Fe}(\text{NO})_2]$ (**5**) (ν_{NO} : 1666 s , 1642 s cm^{-1} in CH_3CN).²⁰ The reduction potential of -1.61 V (vs $\text{FeCp}_2/\text{FeCp}_2^+$) for **3-Et-K** lies between that of complex **5** (-2.264 V vs $\text{FeCp}_2/\text{FeCp}_2^+$) and that of complex $[(\text{NO})_2\text{Fe}(\mu\text{-SEt})_2\text{Fe}(\text{NO})_2]$ (-0.95 V vs $\text{FeCp}_2/\text{FeCp}_2^+$).¹⁸ These results rationalize the trend of the negative reduction potential and the shift of ν_{NO} stretching frequencies to lower energy from complex $[(\text{NO})_2\text{Fe}(\mu\text{-SEt})_2\text{Fe}(\text{NO})_2]$, complex **3**, to complex **5**. Compared to complex **5** and $[(\text{NO})_2\text{Fe}(\mu\text{-SEt})_2\text{Fe}(\text{NO})_2]$, displaying two absorption bands at 264 and 378 nm and at 310 and 360 nm, respectively, in UV-vis spectrum, the anionic mixed thiolate-sulfide-bridged Roussin's red ester **3-Et-K** shows absorption bands at 259, 326, and 376 nm.

Transformation of 3-Et-K into 1-K. In contrast to the inertness of HSCPh_3 toward **3-Et-K**, the addition of 1 equiv of ethylthiolate into a CH_3CN solution of **3-Et-K** and HSCPh_3 under a N_2 atmosphere yielded the known complex **5**, characterized by IR (ν_{NO} stretching frequencies shifting from 1718 and 1693 cm^{-1} to 1666 and 1642 cm^{-1}) and UV-vis (Scheme 1e).²⁰ In comparison, the preliminary study showed that the spontaneous conversion of the anionic mixed thiolate-sulfide-bridged RRE **3-Et** into Roussin's black salt (RBS) occurred upon exposure of complex **3-Et** to O_2 or acid.

When a CH_3CN solution of complex **5** was treated with $[\text{Fe}(\text{SET})_4]^-$ in a 1:2 molar ratio for 10 min at ambient temperature, the appearance of two absorption bands at 456 and 427 nm and the shift of the ν_{NO} stretching frequencies from 1666 s and 1642 s cm^{-1} to 1722 s and 1680 s cm^{-1} confirmed the formation of the known $[\text{K-18-crown-6-ether}]_2[(\text{SET})_2\text{Fe}(\mu\text{-S})_2\text{Fe}(\text{SET})_2]$ (**1-K**) and $[\text{K-18-crown-6-ether}][(\text{NO})_2\text{Fe}(\text{SET})_2]$ (**2-K**). Consistent with the conversion of $[\text{Fe}_4\text{S}_4(\text{NO})_4]^{2-}$ to $[\text{Fe}_4\text{S}_4(\text{SPh})_4]^{2-}$ facilitated by $[\text{Fe}(\text{SPh})_4]^-$,^{15b} the absence of formation of mononitrosyl iron complex $[(\text{NO})\text{Fe}(\text{SET})_3]^-$ suggested that a concerted dinitrosyl-dithiyl radical ($[\text{RS}]^*$) exchange reaction occurred around the Fe center in the transformation of complex **5** into **1-K** and **2-K** triggered by $[\text{Fe}(\text{SET})_4]^-$. Consequently, the conversion of complex **5** back to **1-K** triggered by 2 equiv of complex $[\text{Fe}(\text{SET})_4]^-$ provided a facile pathway for transformation of the NO-modified $[\text{Fe-S}]$ clusters into the original $[\text{Fe-S}]$ clusters via a NO radical-thiyl radical ($[\text{RS}]^*$) exchange reaction.^{15b}

Interconversion between 3-Et-K and $[(\text{NO})_2\text{Fe}(\mu\text{-SPh})(\mu\text{-S})\text{Fe}(\text{NO})_2]$ (3-Ph**).** Transformation of **3-Et-K** to $[\text{K-18-crown-6-ether}][(\text{NO})_2\text{Fe}(\mu\text{-SPh})(\mu\text{-S})\text{Fe}(\text{NO})_2]$ (**3-Ph**)

(20) (a) Thomas, J. T.; Robertson, J. H.; Cox, E. G. *Acta Crystallogr.* **1958**, *11*, 599–604. (b) Sanina, N. A.; Filipenko, O. S.; Aldoshin, S. M.; Ovanesyana, N. S. *Russ. Chem. Bull.* **2000**, *49*, 1109–1112.

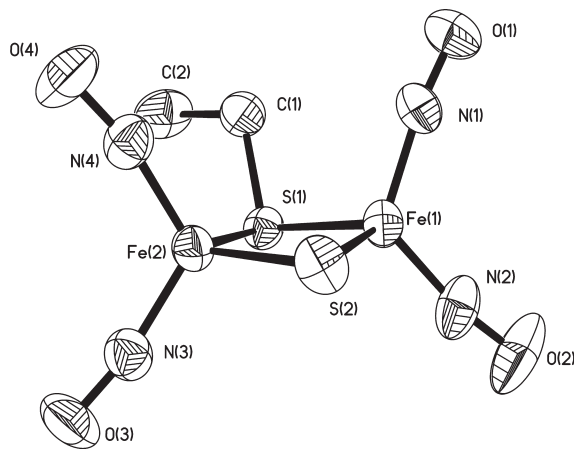


Figure 3. ORTEP drawing and labeling scheme of the $[(\text{NO})_2\text{Fe}(\mu\text{-S})\text{Fe}(\text{NO})_2]^-$ (**3-Et**) unit in $[\text{PPN}]^+$ salt with thermal ellipsoids drawn at 50% probability. Selected bond distances (Å) and angles (deg): $\text{Fe}(1)\cdots\text{Fe}(2)$, 2.6650(9); $\text{Fe}(1)\text{-N}(1)$, 1.670(5); $\text{Fe}(1)\text{-N}(2)$, 1.650(5); $\text{Fe}(2)\text{-N}(3)$, 1.667(5); $\text{Fe}(2)\text{-N}(4)$, 1.674(5); $\text{Fe}(1)\text{-S}(1)$, 2.2455(13); $\text{Fe}(1)\text{-S}(2)$, 2.2280(13); $\text{Fe}(2)\text{-S}(1)$, 2.2510(13); $\text{Fe}(2)\text{-S}(2)$, 2.2317(14); $\text{O}(1)\text{-N}(1)$, 1.173(5); $\text{O}(2)\text{-N}(2)$, 1.177(5); $\text{O}(3)\text{-N}(3)$, 1.171(5); $\text{O}(4)\text{-N}(4)$, 1.170(5); $\text{N}(1)\text{-Fe}(1)\text{-N}(2)$, 118.9(2); $\text{N}(3)\text{-Fe}(2)\text{-N}(4)$, 117.5(2); $\text{N}(1)\text{-Fe}(1)\text{-S}(1)$, 103.86(14); $\text{N}(2)\text{-Fe}(1)\text{-S}(1)$, 107.14(15); $\text{N}(1)\text{-Fe}(1)\text{-S}(2)$, 110.83(14); $\text{N}(2)\text{-Fe}(1)\text{-S}(2)$, 108.65(17); $\text{N}(3)\text{-Fe}(2)\text{-S}(1)$, 109.42(15); $\text{N}(3)\text{-Fe}(2)\text{-S}(2)$, 107.92(14); $\text{N}(4)\text{-Fe}(2)\text{-S}(1)$, 106.43(14); $\text{N}(4)\text{-Fe}(2)\text{-S}(2)$, 108.64(16); $\text{S}(1)\text{-Fe}(1)\text{-S}(2)$, 106.71(5); $\text{S}(1)\text{-Fe}(2)\text{-S}(2)$, 106.40(5); $\text{O}(1)\text{-N}(1)\text{-Fe}(1)$, 168.2(4); $\text{O}(2)\text{-N}(2)\text{-Fe}(1)$, 169.5(5); $\text{O}(3)\text{-N}(3)\text{-Fe}(2)$, 169.4(4); $\text{O}(4)\text{-N}(4)\text{-Fe}(2)$, 167.8(4).

Table 1. Selected Metric Data for Complex **3-Et**, Neutral Roussin's Red Ester, and Roussin's Red Salt²⁰

	$[\text{Fe}(\mu\text{-SEt})(\text{NO})_2]_2$	3-Et	$[\text{Pr}_4\text{N}]_2[\text{Fe}(\mu\text{-S})(\text{NO})_2]_2$
$\text{Fe}\cdots\text{Fe}$ (Å)	2.7080(5)	2.6650(9)	2.704(2)
$\text{Fe}\text{-S}$ (Å) ^a	2.2585(5)	2.2391(14)	2.225(2)
$\text{Fe}\text{-N}$ (Å) ^a	1.6747(11)	1.665(5)	1.653(7)
$\text{N}\text{-O}$ (Å) ^a	1.1708(14)	1.173(5)	1.178(8)
$\text{S}\cdots\text{S}$ (Å)	3.615	3.589	3.535
$\text{Fe}\text{-S}\text{-Fe}$ ∠(deg)	73.671(14)	73.04(4) ^a	74.82(7)
$\text{S}\text{-Fe}\text{-S}$ ∠(deg)	106.329(14)	106.55(5) ^a	105.2(1)
$\text{N}\text{-Fe}\text{-N}$ ∠(deg)	116.10(5)	118.2(2) ^a	111.5(3)
$\text{Fe}\text{-N}\text{-O}$ ∠(deg) ^a	168.4(2)	168.7(5)	163.2(6)
dihedral ∠(deg) ^b	180	171.7	180

^a Average bond distance and angle. ^b Defined by the intersection of the two Fe_2S planes.

was displayed when **3-Et-K** was reacted with 1 equiv of thiophenol in THF (Scheme 1h). The higher-energy ν_{NO} band of complex **3-Ph** (ν_{NO} 1721, 1693 cm^{-1} (THF)) shifted by 6–11 cm^{-1} from that of **3-Et-K** (ν_{NO} 1710, 1687 cm^{-1} (THF)) demonstrated the conversion via phenylthiol protonation. The phenylthiol protonation of the bridged-sulfide ligand of **3-Et-K** and the concurrent nucleophilic attack of phenylthiolate triggering the bridged-ethylthiolate cleavage, and the subsequent elimination of EtSH may rationalize the formation of complex **3-Ph** (Scheme 4). In contrast to thiolates $[\text{RS}]^-$ promoting bridged-thiolate cleavage of RREs $[(\text{NO})_2\text{Fe}(\mu\text{-SEt})_2\text{Fe}(\text{NO})_2]$ to produce DNICs $[(\text{NO})_2\text{Fe}(\text{SR})_2]^-$ and the inertness of complex **5** toward $[\text{RS}]^-$,¹⁸ quantitative transformation of complex **3-Ph** to **3-Et-K** was demonstrated upon the addition of 1 equiv of $[\text{SEt}]^-$ into a THF solution of complex **3-Ph** (Scheme 1h). Presumably, the conversion of the $[\text{Fe}(\mu\text{-SPh})(\mu\text{-S})\text{Fe}]$ core into the $[\text{Fe}(\mu\text{-SEt})(\mu\text{-S})\text{Fe}]$

core is ascribed to the capability of sulfide to bridge the two $\{\text{Fe}(\text{NO})_2\}^9$ fragments and the preference of $\{\text{Fe}(\text{NO})_2\}^9$ motifs to be connected by the stronger electron-donating thiolate. Obviously, the anionic mixed thiolate–sulfide-bridged RREs **3-Et-K** containing the bridged-sulfide–ethylthiolate ligands and complex **3-Ph** containing the bridged-sulfide–phenylthiolate ligands are chemically interconvertible via protonation and a bridged-thiolate exchange reaction, respectively.

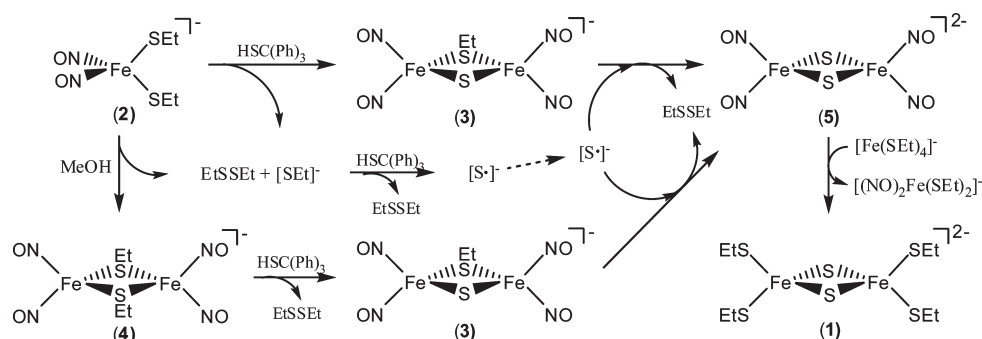
Structure. The single-crystal X-ray structure of the complex **3-Et** unit in the $[\text{PPN}]^+$ salt is depicted in Figure 3, and selected bond dimensions are presented in the figure caption. As shown in Table 1, the geometry of the $[\text{Fe}(\mu\text{-S})(\mu\text{-SEt})\text{Fe}]$ core in complex **3-Et** is best described as a butterfly-like structure with a dihedral angle of 171.7° (the intersection of the two Fe_2S planes) in the solid state. Two nitrosyl groups, bridging sulfide and thiolate, define the distorted tetrahedral geometry of each iron atom, leading to an acute angle $\text{Fe}(1)\text{-S}(1)\text{-Fe}(2)$ of $72.69(4)^\circ$, $\text{Fe}(1)\text{-S}(2)\text{-Fe}(2)$ of $73.39(4)^\circ$, $\text{S}(1)\text{-Fe}(1)\text{-S}(2)$ of $106.71(5)^\circ$, and $\text{S}(1)\text{-Fe}(2)\text{-S}(2)$ of $106.40(5)^\circ$. According to the crystallographic study, complex **3-Me** in $[\text{PPN}]^+$ salt also exhibited a butterfly-like structure with a dihedral angle of 169.2° , similar to complex **3-Et** (Supporting Information, Figure S1). Compared to the $\text{Fe}\text{-N}$ bond distance of 1.6747(11) Å found in complex $[(\text{NO})_2\text{Fe}(\mu\text{-SEt})_2\text{Fe}(\text{NO})_2]$, the shorter $\text{Fe}\text{-N}$ bond distance of 1.665(5) Å observed in complex **3-Et** and 1.653(7) Å observed in complex **5** indicates the better metal π -back-donation to the NO antibonding orbital.²⁰ The mean $\text{N}\text{-O}$ bond distance of 1.173(5) Å in complex **3-Et** is nearly at the upper end of the 1.178(3)–1.160(6) Å range for the anionic $\{\text{Fe}(\text{NO})_2\}^9$ DNICs, and meanwhile, the mean $\text{Fe}\text{-N}(\text{O})$ distance of 1.665(5) Å in complex **3-Et** approaches the lower end of the 1.695(3)–1.661(4) Å range for the anionic $\{\text{Fe}(\text{NO})_2\}^9$ DNICs.²¹ Presumably, the electronic structure of the anionic mixed thiolate–sulfide-bridged Roussin's red esters $[(\text{NO})_2\text{Fe}(\mu\text{-SR})(\mu\text{-S})\text{Fe}(\text{NO})_2]^-$ is best described as $[\{\text{Fe}(\text{NO})_2\}^9-\{\text{Fe}(\text{NO})_2\}^9]$. Furthermore, the strikingly short $\text{Fe}\cdots\text{Fe}$ distance of 2.6650(9) Å observed in complex **3-Et**, compared to 2.7080(5) Å observed in complex $[(\text{NO})_2\text{Fe}(\mu\text{-SEt})_2\text{Fe}(\text{NO})_2]$ and 2.704(2) Å observed in complex **5**, rationalizes the absence of paramagnetism and the EPR signal.

Discussion

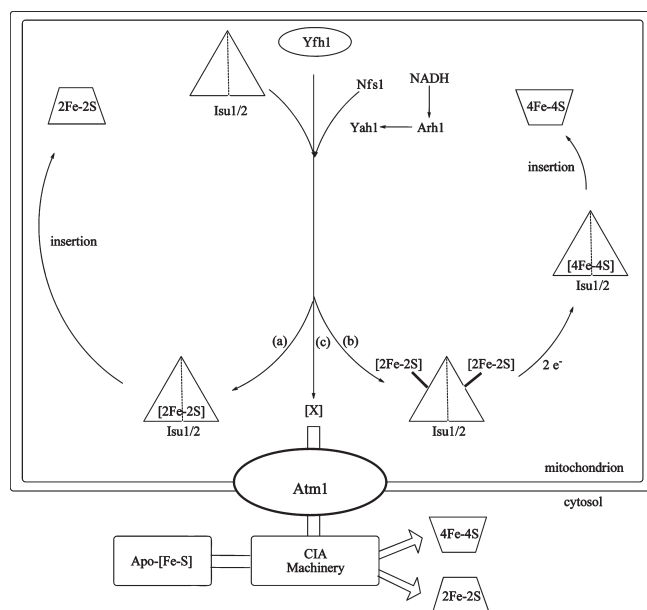
The transformation of DNICs/anionic RREs into the anionic mixed thiolate–sulfide-bridged RREs and the conversion of the anionic mixed thiolate–sulfide-bridged RREs into RRS triggered by the coordinated thiolate(s) of DNICs/anionic RREs demonstrates that the generation of inorganic sulfide occurs via the reduction of triphenylmethanthiol (HSCPh_3 ; Scheme 5). In contrast to the coordinated ethylthiolates of $[(\text{NO})_2\text{Fe}(\text{SEt})_2]^-$ initiating the sulfide release via the reduction of $\text{HSCPh}_3/\text{Me}_2\text{S}_3$, the inertness of $[(\text{NO})_2\text{Fe}(\text{SPh})_2]^-$ toward $\text{HSCPh}_3/\text{Me}_2\text{S}_3$ may signify how the reducing ability of the coordinated cysteinyl ligands of DNICs was regulated by the hydrophobic/hydrophilic environment to modulate the release of sulfide from S-sulfanyl-cysteine in biological systems.

(21) Hung, M.-C.; Tsai, M.-C.; Lee, G.-H.; Liaw, W.-F. *Inorg. Chem.* **2006**, *45*, 6041–6047.

Scheme 5

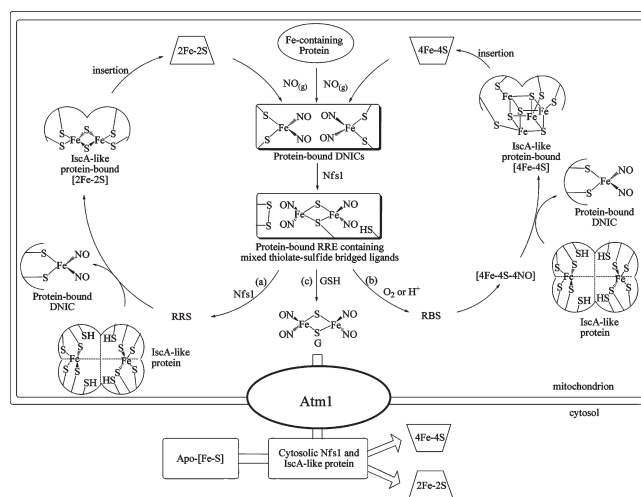


Scheme 6



The biomimetic model study of the reassembling process ($[(\text{NO})_2\text{Fe}(\text{SET})_2]^- / [(\text{NO})_2\text{Fe}(\mu\text{-SET})_2\text{Fe}(\text{NO})_2]^- \rightarrow [(\text{NO})_2\text{Fe}(\mu\text{-S})(\mu\text{-S})\text{Fe}(\text{NO})_2]^- \rightarrow [(\text{SET})_2\text{Fe}(\mu\text{-S})_2\text{Fe}(\text{SET})_2]^{2-} \rightarrow [(\text{SET})_2\text{Fe}(\mu\text{-S})_2\text{Fe}(\text{SET})_2]^{2-}$) may signify the biosynthetic mechanism of the $[2\text{Fe}-2\text{S}]$ cluster. Although the Fe source and the assembling mechanism remain to be investigated, detailed studies of the maturation of $[\text{Fe}-\text{S}]$ proteins in eukaryotes were reported by Lill and Muhlenhoff and by Rouault et al., respectively.^{7,22} As shown in Scheme 6, Fe from Yfh1 incorporating with sulfide, derived from the reduction of S-sulfanyl cysteine of Nfs1 (cysteine desulfurase) by NADH mediated by Yah1 and Arh1, leads to the assembly of an $[\text{Fe}(\mu\text{-S})_2\text{Fe}]$ core. With the aid of Isu1/2 serving as a scaffold protein, the $[\text{Fe}(\mu\text{-S})_2\text{Fe}]$ core finally matures $[2\text{Fe}-2\text{S}]$ proteins (Scheme 6a). Also, reductive coupling of two Isu1/2-bound $[2\text{Fe}-2\text{S}]$ clusters into an Isu1/2-bound $[4\text{Fe}-4\text{S}]$ cluster activates $[4\text{Fe}-4\text{S}]$ iron-sulfur proteins (Scheme 6b).²³ Concerning the maturation of cytosolic $[\text{Fe}-\text{S}]$ proteins, the $[\text{Fe}-\text{S}]$ cluster precursor glutathione-bound $[\text{X}]$ exported by Atm1 to cytosol and further assembled into the $[\text{Fe}-\text{S}]$ cluster by CIA machinery

Scheme 7



was delineated (Scheme 6c).²⁴ It was reported that the participation of cytosolic Isu1 in the assembly of $[\text{Fe}-\text{S}]$ clusters in cytosol could not be excluded since the suppression of cytosolic Isu1 impairs the activation of cytosolic $[\text{Fe}-\text{S}]$ proteins.²⁵

In this model study, the addition of HSCPh_3 and $[\text{SET}]^-$ into the anionic mixed thiolate-sulfide-bridged RREs affords Roussin's red salt under anaerobic conditions, compared to the spontaneous conversion of the anionic mixed thiolate-sulfide-bridged RREs into RBS upon exposure to O_2 or acid.^{15b} These results show that the anionic mixed thiolate-sulfide-bridged RREs act as a key intermediate in the transformation of DNICs into $[2\text{Fe}-2\text{S}]$ and $[4\text{Fe}-4\text{S}]$ clusters, respectively. As shown in Scheme 7a, it is proposed that the insertion of sulfide, derived from the reduction of the S-sulfanyl cysteine of Nfs1 by the pendant cysteinate ligands of DNICs, into DNICs results in the formation of the preassembled protein-bound thiolate-sulfide-containing RREs. The mixed thiolate-sulfide-bridged RREs then react with the cysteinate ligand and cysteine desulfurase to afford RRS under anaerobic conditions. The subsequent NO-radical/thiyl-radical exchange reaction between RRS and rubredoxin-containing proteins (the IscA-like protein) leads to the assembly of a $[2\text{Fe}-2\text{S}]$ cluster to mature $[2\text{Fe}-2\text{S}]$ proteins. Instead, the conversion of the anionic mixed thiolate-sulfide-bridged

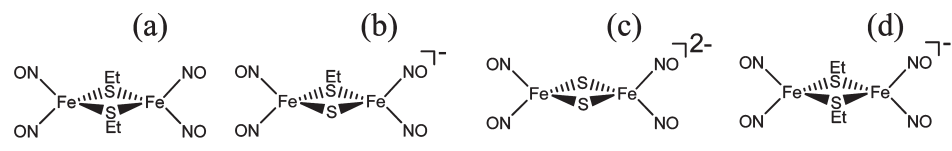
(22) (a) Land, T.; Rouault, T. A. *Mol. Cell* **1998**, *2*, 807–815. (b) Tong, W. H.; Rouault, T. A. *EMBO J.* **2000**, *19*, 5692–5700.

(23) Fontecave, M.; Ollagnier-de-Choudens, S. *Arch. Biochem. Biophys.* **2008**, *474*, 226–237.

(24) (a) Isikawa, T.; Li, Z.-S.; Lu, Y.-P.; Rea, P. A. *Biosci. Rep.* **1997**, *17*, 189–207. (b) Roy, A.; Solodovnikova, N.; Nicholson, T.; Antholine, W.; Walden, W. E. *EMBO J.* **2003**, *22*, 4826–4835.

(25) Tong, W. H.; Rouault, T. A. *Cell Metab.* **2006**, *3*, 199–210.

Chart 1

	(a)	(b)	(c)	(d)
				
Fe...Fe (Å)	2.7080(5)	2.6650(9)	2.704(2)	2.8413(6)
ν_{NO} (cm ⁻¹) ^a	1809 vw, 1774 s, 1749 s	1718 s, 1693 s	1666 s, 1642 s	1675 s, 1658 s
$\Delta\nu_{\text{NO}}$ (cm ⁻¹)	25	25	24	17
Absorption Spectrum (nm) ^a	310, 360	259, 326, 376	264, 378	323, 452, 649, 970
Reduction Potential (V) ^b	-0.95	-1.61	-2.26	-1.61
EPR	silent	Silent	silent	$g_{\perp} = 2.008, g_{\parallel} = 1.968$
Electronic Structure	{Fe(NO) ₂ } ⁹ -{Fe(NO) ₂ } ⁹	{Fe(NO) ₂ } ⁹ -{Fe(NO) ₂ } ⁹	{Fe(NO) ₂ } ⁹ -{Fe(NO) ₂ } ⁹	delocalized {Fe(NO) ₂ } ⁹ -{Fe(NO) ₂ } ¹⁰

RREs into RBS occurs spontaneously in an aerobic environment. The subsequent assembly of [4Fe-4S] clusters in the presence of cysteine desulfurase and rubredoxin-containing proteins activates [4Fe-4S] proteins, as proposed in the previous study (the reassembling process $[(\text{NO})_2\text{Fe}(\mu\text{-SEt})_2]^- / [(\text{NO})_2\text{Fe}(\mu\text{-SEt})_2\text{Fe}(\text{NO})_2]^- \rightarrow [(\text{NO})_2\text{Fe}(\mu\text{-SEt})(\mu\text{-S})\text{Fe}(\text{NO})_2]^- \rightarrow [\text{Fe}_4\text{S}_3(\text{NO})_7]^- / [\text{Fe}_4\text{S}_3(\text{NO})_7]^{2-} \rightarrow [\text{Fe}_4\text{S}_4(\text{NO})_4]^{2-} \rightarrow [\text{Fe}_4\text{S}_4(\text{SEt})_4]^{2-}$; Scheme 7b).^{15b} Additionally, the anionic mixed thiolate-sulfide-bridged RREs produced in mitochondria may be transformed into the anionic mixed GS-sulfide-bridged RREs. The anionic mixed GS-sulfide-bridged RREs are then exported to cytosol via Atm1 for further assembling into [2Fe-2S]/[4Fe-4S] clusters by cytosolic cysteine desulfurase and rubredoxin-containing proteins (Scheme 7c).²⁴ On the basis of this study, the protein-bound RREs containing the bridging thiolate-sulfide ligands were proposed to be a key intermediate in determining the biosynthesis of [2Fe-2S] and [4Fe-4S] iron-sulfur proteins.

Conclusion and Comments

Studies on the transformation of DNICs to [2Fe-2S] clusters via the anionic mixed thiolate-sulfide-bridged intermediate $[(\text{NO})_2\text{Fe}(\mu\text{-SR})(\mu\text{-S})\text{Fe}(\text{NO})_2]^-$ and on the reactivity of the anionic mixed thiolate-sulfide-bridged RREs have resulted in the following results:

- (1) The anionic mixed thiolate-sulfide-bridged RREs $[(\text{NO})_2\text{Fe}(\mu\text{-SR})(\mu\text{-S})\text{Fe}(\text{NO})_2]^-$ (R = Et, Me and Ph) containing a {Fe(NO)₂}⁹-{Fe(NO)₂}⁹ core were synthesized and characterized by IR, UV-vis, EPR, ¹H NMR, and cyclic voltammetry

as well as single-crystal X-ray diffraction. To the best of our knowledge, the dinuclear dinitrosyl iron complexes can then be classified into (a) the neutral RREs,^{20a} (b) the anionic mixed thiolate-sulfide-bridged RREs, (c) RRS,^{20b} and (d) the anionic RREs,¹⁸ as shown in Chart 1.

- (2) Compared to the inertness of RRS $[\text{Fe}(\mu\text{-S})(\text{NO})_2]_2^{2-}$ toward $[\text{RS}]^-$ (R = Et, Ph), the addition of $[\text{EtS}]^-$ into RRE $[(\text{NO})_2\text{Fe}(\mu\text{-SEt})_2\text{Fe}(\text{NO})_2]^-$ producing DNIC $[(\text{NO})_2\text{Fe}(\text{SEt})_2]^-$ via bridged-thiolate cleavage was reported.¹⁸ In contrast, the addition of the stronger electron-donating ethylthiolate $[\text{EtS}]^-$ into the anionic mixed phenylthiolate-sulfide-bridged RRE **3-Ph** triggers a bridged-thiolate exchange reaction to yield **3-Et**. This result clearly demonstrates that the dinuclear {Fe(NO)₂}⁹-{Fe(NO)₂}⁹ motif prefers the stronger electron-donating sulfide and alkylthiolate over phenylthiolate. Reversibly, protonation of the anionic mixed ethylthiolate-sulfide-bridged RRE **3-Et** by PhSH induces the bridged-thiolate exchange reaction to yield **3-Ph**. These results show that the anionic mixed thiolate-sulfide-bridged RREs $[(\text{NO})_2\text{Fe}(\mu\text{-SR})(\mu\text{-S})\text{Fe}(\text{NO})_2]^-$ containing the different bridged thiolates are chemically interconvertible via thiol protonation and a thiolate-exchange reaction, respectively.
- (3) In contrast to the nucleophilicity (reducing ability) displayed by **2-PPN**, the inertness of $[\text{PPN}]^-$ - $[(\text{NO})_2\text{Fe}(\text{SPh})_2]$ toward HSCPh_3 implicates how

the reducing ability of the coordinated thiolates of DNICs modulates the release of sulfide from HSCPh₃ via reduction accompanied by the concurrent conversion of DNICs into the anionic mixed-sulfide–thiolate-bridged complex.

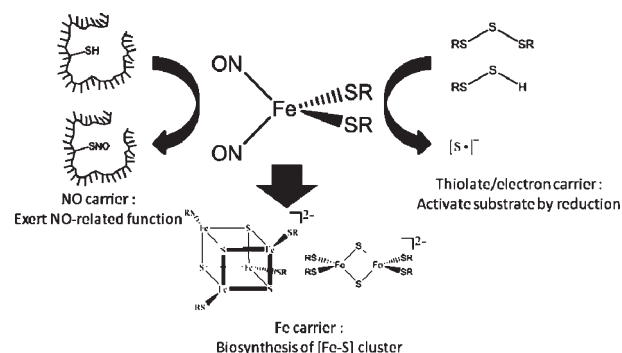
- (4) The transformation of DNICs into [2Fe–2S] clusters facilitated by HSCPh₃ or Me₂S₃ via the reassembling process $[(\text{NO})_2\text{Fe}(\text{SEt})_2]^- / [(\text{NO})_2\text{Fe}(\mu\text{-SEt})_2\text{Fe}(\text{NO})_2]^- \rightarrow [(\text{NO})_2\text{Fe}(\mu\text{-SEt})(\mu\text{-S})\text{Fe}(\text{NO})_2]^- \rightarrow [(\text{NO})_2\text{Fe}(\mu\text{-S})_2\text{Fe}(\text{NO})_2]^{2-} \rightarrow [(\text{S-Et})_2\text{Fe}(\mu\text{-S})_2\text{Fe}(\text{SEt})_2]^{2-}$ was consistent with the repair of DNICs back to the ferredoxin [2Fe–2S] cluster by cysteine desulfurase (IscS) and L-cysteine in vitro with no need of the addition of iron or any other protein components in *E. coli*.¹³

DNICs are known as one possible naturally occurring form for the storage and transport of nitric oxide in biological systems to exert NO-related functions, for example, S-nitrosylation of HSP70 transcriptional factor (HSF), triggering trimerization and the activation of HSF to induce accumulation of HSP70.^{6,26} Presumably, the thiolate-coordinate DNICs serve as not only the thiolate/electron carrier activating the incorporation of sulfide to assemble an [Fe(μ-S)₂Fe] core but also the Fe carrier/source in the biosynthesis of [2Fe–2S] and [4Fe–4S] iron–sulfur clusters (Scheme 8). Since [Fe–S] proteins have been known to have a critical influence on the uptake, intracellular distribution, and utilization of iron, this biomimetic study supports the position that DNICs may regulate Fe uptake and cellular iron homeostasis.^{1,7}

Experimental Section

Manipulations, reactions, and transfers were conducted under nitrogen according to Schlenk techniques or in a glove-box (N₂ gas). Solvents were distilled under nitrogen from appropriate drying agents (diethyl ether from CaH₂; acetonitrile from CaH₂–P₂O₅; methylene chloride from CaH₂; methanol from Mg/I₂; hexane and tetrahydrofuran (THF) from sodium benzophenone) and stored in dried, N₂-filled flasks over 4 Å molecular sieves. Nitrogen was purged through these solvents before use. Solvent was transferred to the reaction vessel via stainless cannula under positive pressure of N₂. Complexes [K-18-crown-6-ether][(NO)₂Fe(μ-SEt)₂Fe(NO)₂],¹⁸ [PPN][(NO)₂Fe(SEt)₂],¹⁸ [PPN][Fe(SEt)₄], and [PPN]₂[(SEt)₂Fe(μ-S)₂Fe(SEt)₂] were synthesized on the basis of the reported literature.²⁷ The reagents PPh₃ (Wako), methyltrisulfide (Acros), and HSCPh₃ and HSPH (Aldrich) were used as-received. The NO(g) (SanFu, 10% NO + 90% N₂) was passed through an Ascarite II column to remove higher nitrogen oxides before use.²⁸ Infrared spectra of the ν_{NO} stretching frequencies were recorded on a PerkinElmer model spectrum One B spectrometer with sealed solution cells (0.1 mm, CaF₂ windows). UV–vis spectra were recorded on a Jasco V-570 spectrometer. Electrochemical measurements were performed with CHI model 421 potentiationstat (CH Instrument) instrumentation. Cyclic voltammograms were obtained from a 10 mM analyte concentration in O₂-free

Scheme 8



CH₃CN using 0.2 M [*n*-Bu₄N][PF₆] as a supporting electrolyte. The potential was measured at 298 K versus a Ag/AgCl reference electrode by using a glassy carbon working electrode. ¹H and ³¹P NMR spectra were obtained on a Varian Unity-500 spectrometer. Analyses of carbon, hydrogen, and nitrogen were obtained with a CHN analyzer (Heraeus).

Reaction of [PPN]₂[(SEt)₂Fe(μ-S)₂Fe(SEt)₂] (1-PPN) and Nitric Oxide under the Presence of PPh₃. Under a N₂ atmosphere, to a CH₃CN solution (3 mL) of triphenylphosphine (0.026 g, 0.1 mmol) and [PPN]₂[(SEt)₂Fe(μ-S)₂Fe(SEt)₂] (1-PPN) (0.085 g, 0.05 mmol) was added NO(g) (48 mL (10% NO + 90% N₂), 0.2 mmol) via a gastight syringe at 0 °C. The reaction solution was stirred and monitored by FTIR immediately. The IR ν_{NO} spectrum displaying two strong stretching bands at 1722 and 1680 cm⁻¹ was consistent with the formation of [PPN][(NO)₂Fe(SEt)₂] (2-PPN). The addition of diethyl ether to the THF solution led to the precipitation of red-brown solid 2-PPN (yield: 0.069 g, 89%), characterized by IR and UV–vis. Evaporation of the THF–diethyl ether solution yielded S=PPh₃, identified by ³¹P NMR (δ 42.70 ppm in CH₃CN).

Conversion of 2-PPN into [PPN][(NO)₂Fe(μ-SEt)(μ-S)Fe(NO)₂] (3-Et). HSCPh₃ (0.055 g, 0.2 mmol) and 2-PPN (0.310 g, 0.4 mmol) were dissolved in CH₃CN (5 mL) and stirred under N₂ at 0 °C for 1 h. The reaction solution was then stirred overnight at ambient temperature and monitored with FTIR. An IR ν_{NO} shift from 1722 s and 1680 s cm⁻¹ to 1718 s and 1693 s cm⁻¹ was observed. The mixture solution was dried under a vacuum, and the crude solid was redissolved in THF (5 mL). Then, the solution was filtered through Celite to remove the insoluble [PPN][SEt] solid characterized by ¹H NMR (δ 7.79 (m), 7.46 (m), 2.37 (q), 1.13 (t) ppm in CD₃CN). The addition of hexane (20 mL) to the filtrate (THF solution) led to the precipitation of brown solid [PPN][(NO)₂Fe(μ-SEt)(μ-S)Fe(NO)₂] (3-Et) (yield: 0.136 g, 79%). The upper solution (THF–hexane solution) was dried under a vacuum to obtain EtSSEt (δ 2.70 (q), 1.27 (t) ppm in CD₃CN) and HC(Ph)₃ (δ 7.29 (m), 7.21 (m), 7.13 (m), 5.59 (s) ppm in CD₃CN), characterized by ¹H NMR. Dark-brown crystals suitable for X-ray diffraction analysis were isolated from a THF solution of complex 3-Et layered by hexane in a tightly sealed flask. IR ν_{NO}: 1709 s, 1686 s cm⁻¹ (THF); 1718 s, 1693 s cm⁻¹ (CH₃CN). Absorption spectrum (THF) [nm, λ_{max}(M⁻¹ cm⁻¹, ε)]: 259 (8600), 326 (4100), 376 (5100). ¹H NMR (CD₃CN): δ 7.81 (m), 7.49 (m), 2.71 (q), 1.40 (t) ppm. Anal. Calcd for C₃₈H₃₅Fe₂N₅O₄P₂S₂: C, 52.86; H, 4.09; N, 8.11. Found: C, 52.11; H, 4.20; N, 7.83.

Transformation of 2-PPN into [PPN][(NO)₂Fe(μ-SMe)(μ-S)Fe(NO)₂] (3-Me). Compounds methyltrisulfide (0.025 g, 0.2 mmol) and 2-PPN (0.310 g, 0.4 mmol) were dissolved in CH₃CN (5 mL) and stirred at 0 °C under N₂. The reaction was monitored with FTIR, and an IR ν_{NO} shift from 1722 s and 1680 s cm⁻¹ to 1719 s and 1697 s cm⁻¹ was observed. After being stirred for 1 h, diethyl ether (15 mL) was added, and the mixture solution was filtered through Celite to remove the [PPN][SMe] (δ 7.82 (m),

(26) Chen, Y.-C.; Ku, W.-C.; Feng, L.-T.; Tsai, M.-L.; Hsieh, C.-H.; Hsu, W.-H.; Liaw, W.-F.; Hung, C.-H.; Chen, Y.-J. *J. Am. Chem. Soc.* **2008**, *130*, 10929–10938.

(27) (a) Maelia, L. E.; Millar, M.; Koch, S. A. *Inorg. Chem.* **1992**, *31*, 4594–4600. (b) Han, S.; Czernuszewicz, R. S.; Spiro, T. G. *Inorg. Chem.* **1986**, *25*, 2276–2277.

(28) Works, C. F.; Jocher, C. J.; Bart, G. D.; Bu, X.; Ford, P. C. *Inorg. Chem.* **2002**, *41*, 3728–3739.

7.49 (m), 2.19 (s) ppm in CD₃CN). Then, hexane was added into the filtrate to precipitate [PPN][(NO)₂Fe(*μ*-SMe)(*μ*-S)Fe(NO)₂] (**3-Me**) (yield: 0.136 g, 79%). Byproduct diethyl disulfide dissolved in the THF–diethyl ether–hexane solution was isolated and characterized by ¹H NMR. Recrystallization from THF solution of complex **3-Me** layered with diethyl ether at –20 °C for 4 days led to dark brown crystals suitable for X-ray crystallography. IR ν_{NO} : 1709 s, 1688 s cm⁻¹ (THF); 1719 s, 1697 s cm⁻¹ (CH₃CN). Absorption spectrum (CH₃CN) [nm, λ_{max} (M⁻¹ cm⁻¹, ϵ): 253 (9000), 295 (4500), 377 (5500)]. ¹H NMR (CD₃CN): δ 7.79 (m), 7.45 (m), 2.46 (s) ppm. Calcd for C₃₇H₃₃Fe₂N₅O₄P₂S₂: C, 52.32; H, 3.92; N, 8.24. Found: C, 52.51; H, 4.12; N, 8.63.

Transformation of [K-18-crown-6-ether][(NO)₂Fe(*μ*-SEt)₂Fe(NO)₂] (4**) into [K-18-crown-6-ether][(NO)₂Fe(*μ*-SEt)(*μ*-S)Fe(NO)₂] (**3-Et-K**).** To a 30 mL Schlenk flask loaded with [K-18-crown-6-ether][(NO)₂Fe(*μ*-SEt)₂Fe(NO)₂] (**4**) (0.071 g, 0.1 mmol) and HSCPh₃ (0.0276 g, 0.1 mmol; or Me₂S₃ (0.013 g, 0.1 mmol)) was added THF (3 mL). The reaction solution was stirred under N₂ at ambient temperature overnight and monitored by FTIR. An IR ν_{NO} shift from 1673 s and 1655 s cm⁻¹ to 1710 s and 1687 s cm⁻¹ was observed. Hexane was then added to lead to the precipitation of the brown solid [K-18-crown-6-ether][(NO)₂Fe(*μ*-SEt)(*μ*-S)Fe(NO)₂] (**3-Et-K**; yield 0.054 g, 86%). Byproducts EtSSEt and HC(Ph)₃ dissolved in a THF–hexane solution were isolated and characterized by ¹H NMR. In a similar fashion, the reaction of complex **4** and Me₂S₃ led to the formation of **3-Et-K** accompanied by the byproducts EtSSEt and MeSSMe (δ 2.40 (s) ppm in CD₃CN), characterized by ¹H NMR. IR ν_{NO} : 1710 s, 1687 s cm⁻¹ (THF); 1718 s, 1693 s cm⁻¹ (CH₃CN). Absorption spectrum (THF) [nm, λ_{max} (M⁻¹ cm⁻¹, ϵ): 259 (8600), 326 (4300), 376 (5200)]. ¹H NMR (CD₃CN): δ 3.56 (s) (18-crown-6-ether), 2.71 (q), 1.40 (t) ppm (SEt).

Transformation of 3-Et-K into [K-18-crown-6-ether]₂[(NO)₂Fe(*μ*-S)₂Fe(NO)₂] (5**).** A CH₃CN solution (5 mL) of **3-Et-K** (0.126 g, 0.2 mmol) was transferred to a 30 mL Schlenk flask loaded with HSCPh₃ (0.055 g, 0.2 mmol), [K][SEt] (0.020 g, 0.2 mmol), and 18-crown-6-ether (0.053 g, 0.2 mmol) under a positive N₂ atmosphere. The reaction solution was stirred overnight and monitored by FTIR. An IR ν_{NO} shift from 1718 s and 1693 s cm⁻¹ to 1666 s and 1642 s cm⁻¹ was observed. The addition of diethyl ether into the CH₃CN mixture solution led to the precipitation of the known [K-18-crown-6-ether]₂[(NO)₂Fe(*μ*-S)₂Fe(NO)₂] (**5**; yield 0.148 g, 82%), characterized by IR and UV–vis.^{20b} Byproducts EtSSEt and HC(Ph)₃ dissolved in the CH₃CN–diethyl ether solution were isolated and characterized by ¹H NMR.

Reaction of Complex 5 and [K-18-crown-6-ether][Fe(SEt)₄]. CH₃CN solution (2 mL) of complex **5** (0.045 g, 0.1 mmol) was added to the CH₃CN solution of [K-18-crown-6-ether][Fe(SEt)₄] (0.121 g, 0.2 mmol) in a dropwise manner at ambient temperature. The reaction was monitored by FTIR. After the reaction solution was stirred for 1 h, the IR ν_{NO} shifting from 1666 s, 1642 s cm⁻¹ to 1722 s, 1680 s cm⁻¹ implicated the formation of [K-18-crown-6-ether][(NO)₂Fe(SEt)₂] (**2-K**). Diethyl ether was added into the CH₃CN solution to separate the known red-brown precipitate [K-18-crown-6-ether]₂[(SEt)₂Fe(*μ*-S)₂Fe(SEt)₂] (**1-K**; yield 0.048 g, 47%), identified by

UV–vis,²⁷ and the yellow-brown upper solution. The upper solution (CH₃CN–diethyl ether solution) was dried under a vacuum and redissolved in THF. The yellow-brown solution was filtered through Celite to remove the insoluble solid. The addition of hexane into the filtrate led to the precipitation of red-brown solid **2-K**, characterized by FTIR and UV–vis.

Conversion of 3-Et-K into [K-18-crown-6-ether][(NO)₂Fe(*μ*-SPh)(*μ*-S)Fe(NO)₂] (3-Ph**).** To the THF solution (3 mL) of **3-Et-K** (0.063 g, 0.1 mmol) was added HSPH (0.011 g, 0.1 mmol) at 0 °C. After the mixture solution was stirred at 0 °C for 1 h, the reaction solution was further stirred overnight at ambient temperature. The reaction was monitored with FTIR, and an IR ν_{NO} shift from 1710 s and 1687 s cm⁻¹ to 1721 s and 1693 s cm⁻¹ was observed. Hexane was then added to the THF solution (3 mL), leading to the precipitation of complex **3-Ph** (yield: 0.059 g, 88%). IR ν_{NO} : 1721 s, 1693 s cm⁻¹ (THF). Absorption spectrum (THF) [nm, λ_{max} (M⁻¹ cm⁻¹, ϵ): 271 (7500), 379 (5000)]. ¹H NMR (CD₃CN): δ 7.3 (m), 3.52 (s) ppm.

Transformation of Complex 3-Ph into 3-Et-K. Complexes **3-Ph** (0.068 g, 0.1 mmol) and [K][SEt] (0.18 g, 0.3 mmol) were dissolved in THF (5 mL) under a N₂ atmosphere. The mixture solution was stirred for 10 min at ambient temperature and monitored by FTIR. The IR ν_{NO} spectrum displaying strong stretching bands at 1710 s and 1687 s cm⁻¹ (THF) shows the formation of **3-Et-K**. Diethyl ether (5 mL) was added to the mixture solution, and then the mixture solution was filtered to remove the insoluble [K][SPh]. Hexane was added to the filtrate to precipitate **3-Et-K** (yield: 0.057 g, 90%), characterized by IR and UV–vis.

Crystallography. Crystallographic data and structure refinement parameters of complexes **3-Et** and **3-Me** are summarized in the Supporting Information. The crystal chosen for X-ray diffraction studies measured 0.45 × 0.4 × 0.35 mm for complex **3-Et** and 0.42 × 0.18 × 0.02 mm for complex **3-Me**. The crystal was mounted on a glass fiber and quickly coated in epoxy resin. Unit cell parameters were obtained by least-squares refinement. Diffraction measurements for complexes **3-Et** and **3-Me** were carried out on a Kappa CCD diffractometer with graphite-monochromated Mo K α radiation ($\lambda = 0.7107 \text{ \AA}$) between 2.25° and 25.37° for complex **3-Et** and between 1.29° and 25.03° for complex **3-Me**. Least-squares refinements of the positional and anisotropic thermal parameters of all non-hydrogen atoms and hydrogen atoms were fixed at calculated positions and refined as riding modes. A multiscan absorption correction was made. The SHELXTL²⁹ structure refinement program was employed.

Acknowledgment. We gratefully acknowledge financial support from the National Science Council of Taiwan. The authors thank Mr. Ting-Shen Kuo for single-crystal X-ray structural determinations.

Supporting Information Available: X-ray crystallographic files in CIF format for the structure determinations of [PPN][(NO)₂Fe(*μ*-SEt)(*μ*-S)Fe(NO)₂] and [PPN][(NO)₂Fe(*μ*-SMe)(*μ*-S)Fe(NO)₂]. This material is available free of charge via the Internet at <http://pubs.acs.org>.

(29) Sheldrick, G. M. *SHELXTL*; Siemens Analytical X-ray Instruments Inc.: Madison, WI, 1994.